

Implementing fault-tolerant non-Clifford gates using the $[[8,3,2]]$ color code

Daniel Honciuc Menendez,¹ Annie Ray,^{2,3} and Michael Vasmer^{2,3}

¹*Department of Physics, University of Toronto, Toronto, ON M5S 1A7, Canada*

²*Institute for Quantum Computing, University of Waterloo, Waterloo, ON N2L 3G1, Canada*

³*Perimeter Institute for Theoretical Physics, Waterloo, ON N2L 2Y5, Canada*

(Dated: August 1, 2025)

Quantum computers promise to solve problems that are intractable for classical computers, but qubits are vulnerable to many sources of error, limiting the depth of the circuits that can be reliably executed on today's quantum hardware. Quantum error correction has been proposed as a solution to this problem, whereby quantum information is protected by encoding it into a quantum error-correcting code. But protecting quantum information is not enough, we must also process the information using logic gates that are robust to faults that occur during their execution. One method for processing information fault-tolerantly is to use quantum error-correcting codes that have logical gates with a tensor product structure (transversal gates), making them naturally fault-tolerant. Here, we test the performance of a code with such transversal gates, the $[[8,3,2]]$ color code, using trapped-ion and superconducting hardware. We observe improved performance (compared to no encoding) for encoded circuits implementing non-Clifford gates, a class of gates that are essential for achieving universal quantum computing. In particular, we find improved performance for an encoded circuit implementing the control-control Z gate, a key gate in Shor's algorithm. Our results illustrate the potential of using codes with transversal gates to implement non-trivial algorithms on near-term quantum hardware.

I. INTRODUCTION

Quantum error correction (QEC) promises to unlock the full potential of quantum computing, by protecting fragile qubits from the effects of decoherence [1–3]. But it is not enough to merely preserve the quantum information stored in a qubit register, we also need to perform a universal set of logical gates in a fault-tolerant manner [4]. Logical gates in the Clifford group (the unitaries that map Pauli operators to Pauli operators) are often relatively straightforward to implement fault-tolerantly in a given QEC code, however they are not universal. In fact, no QEC code can have a transversal and universal set of logical gates [5]. To obtain a universal gate set we need an additional non-Clifford gate [6], but implementing gates from this class fault-tolerantly is often difficult, usually requiring complex procedures such as magic state distillation [7, 8].

Certain QEC codes with special structure have transversal non-Clifford gates, where a transversal gate is a gate that acts as a tensor product unitaries that do not entangle different qubits in the same QEC code block. Examples of such gates include the transversal CNOT available in all CSS codes, and any gate acting as a tensor product of single-qubit unitaries. Transversal gates are naturally fault-tolerant as they do not spread errors within a code block.

There exists a family of codes known as triorthogonal codes [9] with transversal non-Clifford gates, implemented by tensor products of $T = \text{diag}(1, \exp(i\pi/4))$. Certain (generalized) triorthogonal codes have transversal entangling non-Clifford gates, the smallest of which (to our knowledge) is the $[[8,3,2]]$ color code [10, 11], which has a transversal $\text{CCZ} = \text{diag}(1, 1, 1, 1, 1, 1, 1, -1)$ gate. From a fault-tolerance perspective, it is particularly

desirable to implement complex entangling gates using single-qubit gates, as single-qubit gates are often an order of magnitude less noisy than entangling gates in many hardware platforms [12–17]. Using small codes to demonstrate fault-tolerant Clifford and non-Clifford operations has previously been suggested [18] and implemented in NMR [19, 20], trapped-ion [21–24], and superconducting hardware [25–27].

Here, we investigate the performance of the encoded gates of the $[[8,3,2]]$ code on superconducting and trapped-ion hardware platforms. We compare the performance of the encoded gates with the same gates executed with no encoding, finding that the encoded gates perform better than their bare (non-encoded) counterparts in every case where the encoded gate is non-Clifford, even though the encoded circuits contain more entangling gates than the bare circuits. Notably, we observe improved performance for the CCZ gate, which is the dominant gate in circuits such as adders [28, 29] and the modular exponentiation used in Shor's algorithm [30, 31].

The remainder of this article is structured as follows. In Section II, we review the definition of the $[[8,3,2]]$ code and its transversal logical gates. In Section III, we give fault-tolerant circuits for preparing encoded states of the $[[8,3,2]]$ code and for logical measurements. In Section IV, we describe our demonstrations on quantum hardware and their results, and we conclude with Section V.

II. THE $[[8,3,2]]$ COLOR CODE

The $[[8,3,2]]$ color code is a stabilizer code [32], encoding 3 logical qubits into 8 physical qubits with distance 2 (meaning that it can detect any single-qubit error). It is convenient to define the code using a geometric represen-

tation, where the physical qubits reside at the vertices of a cube, as shown in Fig. 1. The stabilizer group is generated by an X -type operator acting on all the qubits, and by Z -type operators associated with the faces of the cube. Concretely, using the qubit indices in Fig. 1, the stabilizer group is

$$\mathcal{S} = \langle X^{\otimes 8}, Z_0 Z_1 Z_2 Z_3, Z_4 Z_5 Z_6 Z_7, Z_0 Z_1 Z_4 Z_5, Z_0 Z_2 Z_4 Z_6 \rangle, \quad (1)$$

where Z_i denotes a Pauli Z operator acting on qubit i etc. We note that the stabilizer generators in Eq. (1) are either X -type or Z -type, meaning that the $[[8,3,2]]$ code is a CSS code [33, 34].

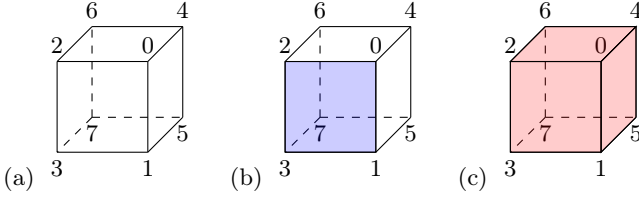


Figure 1. Geometric representation of the $[[8,3,2]]$ code. (a) The physical qubits reside at the vertices of the cube. (b) Z -type stabilizers are associated with faces, for example the blue face has an associated stabilizer $Z_0 Z_1 Z_2 Z_3$. (c) The X -type stabilizer acts on all the qubits.

The logical operators of the $[[8,3,2]]$ code also have a geometric interpretation. Logical X operators are associated with the faces of the cube, and logical Z operators with the edges of the cube. We can choose the following basis of logical Pauli operators

$$\begin{aligned} \overline{X}_1 &= X_0 X_1 X_2 X_3, & \overline{Z}_1 &= Z_0 Z_4, \\ \overline{X}_2 &= X_0 X_1 X_4 X_5, & \overline{Z}_2 &= Z_0 Z_2, \\ \overline{X}_3 &= X_0 X_2 X_4 X_6, & \overline{Z}_3 &= Z_0 Z_1, \end{aligned} \quad (2)$$

where we use overlines to distinguish operators acting on the logical qubits from operators acting on the physical qubits.

The $[[8,3,2]]$ code is notable for having a non-Clifford transversal gate, CCZ implemented by T and T^\dagger gates. Specifically,

$$\overline{\text{CCZ}} = T_0 T_1^\dagger T_2^\dagger T_3 T_4^\dagger T_5 T_6 T_7^\dagger. \quad (3)$$

This gate again has a geometric interpretation: vertices and edges of the cube form a bipartite graph and CCZ is implemented by applying T to (the qubits on) one set of the vertices and T^\dagger to the other. The transversality of CCZ and Pauli X imply that the $[[8,3,2]]$ code also has transversal $\text{CZ} = \text{diag}(1, 1, 1, -1)$ gates, as follows

$$\begin{aligned} \overline{\text{CZ}}_{12} &= S_0 S_2^\dagger S_4^\dagger S_6, \\ \overline{\text{CZ}}_{13} &= S_0 S_1^\dagger S_4^\dagger S_5, \\ \overline{\text{CZ}}_{23} &= S_0 S_1^\dagger S_2^\dagger S_3, \end{aligned} \quad (4)$$

where $S = T^2$ and CZ_{ij} acts on logical qubits i and j .

III. FAULT-TOLERANT CIRCUITS

For an error-detecting code such as the $[[8,3,2]]$ code, we say that a circuit is fault-tolerant if any single-qubit error on the input state or an error at any single location in the circuit can at worst lead to a detectable error on the output state. A circuit location can be a state preparation, gate, or measurement. We need only consider Pauli errors due to error discretization [35]. And we note that as the $[[8,3,2]]$ code is a CSS code, it is sufficient to analyse X and Z errors independently. We remark that the logical CCZ and CZ gates discussed in Section II are transversal and are therefore trivially fault-tolerant. We also need fault-tolerant circuits for logical measurement and logical state preparation, and we now discuss each of these in turn.

As the $[[8,3,2]]$ code is a CSS code, we can do a fault-tolerant measurement of the logical qubits in the X or Z basis by measuring all of the physical qubits in the X or Z basis, respectively, and processing the classical outcomes [35]. In the case of an error-detecting code such as the $[[8,3,2]]$ code, the classical processing is especially simple: we simply discard any measurement result that corresponds to a state that is not a $+1$ eigenvalue of the stabilizers. For example, when measuring in the X basis we accept any result whose parity is even, i.e., a $+1$ eigenstate of $X^{\otimes 8}$. This is fault-tolerant because single-qubit errors before the measurements are detectable by definition, and any single measurement error is equivalent to a single-qubit error before the measurement.

A. GHZ state preparation

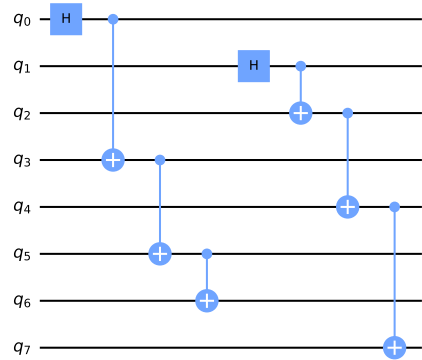


Figure 2. Fault-tolerant circuit for preparing the $|\text{GHZ}\rangle$ state in the $[[8,3,2]]$ code.

First we consider a fault-tolerant circuit for preparing the logical GHZ state, $|\text{GHZ}\rangle = (|000\rangle + |111\rangle)/\sqrt{2}$. Our circuit (shown in Fig. 2) factorizes into two independent and identical sub-circuits acting on qubits 0, 3, 5, 6 and qubits 1, 2, 4, 7 (the two bipartite sets discussed in Section II). The $[[8,3,2]]$ code can detect any

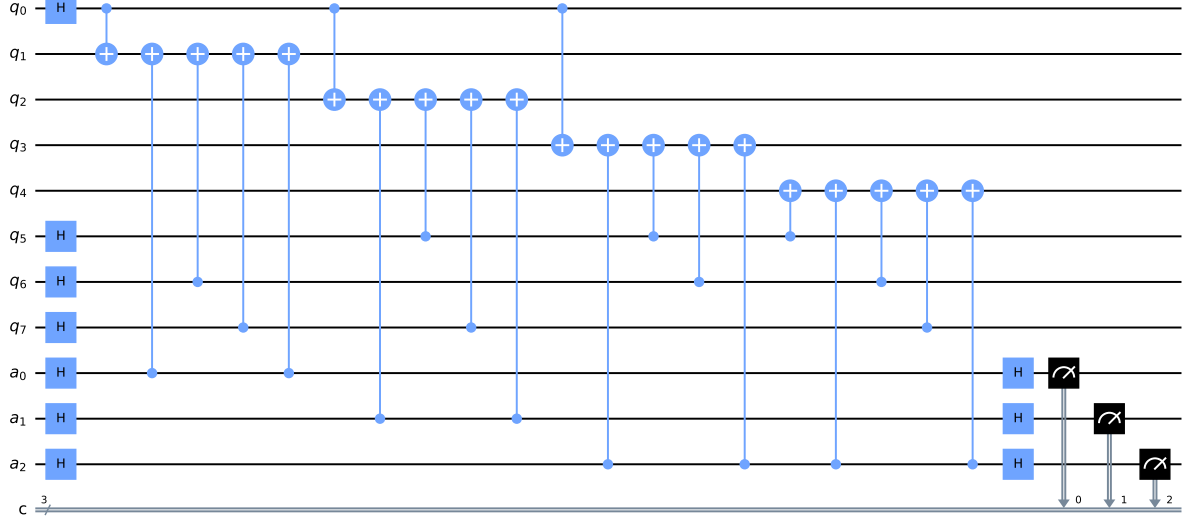


Figure 3. Fault-tolerant circuit for preparing the state $|+++ \rangle$ in the $[[8,3,2]]$ code. The qubits a_1 , a_2 and a_3 are flag qubits whose purpose is to detect certain Z errors that could cause logical errors. If we measure the three flag qubits to be in the $|0\rangle$ state then we accept the output.

weight ≤ 3 X error and so we only need to consider the four-qubit errors $X_0X_3X_5X_6$ and $X_1X_2X_4X_7$. However, each of these errors is in fact a logical $\bar{X}_1\bar{X}_2\bar{X}_3$ operator and so leaves the target $|\text{GHZ}\rangle$ state invariant. The only possible Z errors are weight one (detectable) and weight two (non-detectable). However, one can verify that all the non-detectable errors have trivial action on the target $|\text{GHZ}\rangle$ state. For example, the first CNOT could fail giving a Z_1Z_2 error, but this implements a logical $\bar{Z}_2\bar{Z}_3$ operator (see Eq. (2)) and hence leaves the target $|\text{GHZ}\rangle$ state invariant.

B. $|+++ \rangle$ state preparation

Next, we provide a fault-tolerant circuit for preparing the $|+++ \rangle$ state, shown in Fig. 3. In this circuit, the potentially problematic errors are those that can propagate through the CNOT gates. Consider, for example, the CNOT gates with qubit 0 as the control. The possible multi-qubit X errors that can arise from these gates are

$$\begin{aligned} X_0X_3 & \text{ (detectable),} \\ X_0X_2X_3 & \text{ (detectable),} \\ X_0X_1X_2X_3 & (\bar{X}_1), \end{aligned} \quad (5)$$

where the only non-detectable error has trivial action on the target encoded state. The same is true for the other groups of CNOT gates with the same target. Certain Z errors can also propagate through CNOT gates. For example, consider the CNOT gates with qubit 1 as the target. The possible multi-qubit Z errors that can arise

from these gates are

$$\begin{aligned} Z_1Z_{a_0} & \text{ (detectable),} \\ Z_1Z_7Z_{a_0} & \text{ (detectable),} \\ Z_1Z_6Z_7 & \text{ (detectable),} \\ Z_1Z_6Z_7Z_{a_0} & \text{ (detectable),} \\ Z_0Z_1Z_6Z_7 & \text{ (stabilizer).} \end{aligned} \quad (6)$$

The purpose of the flag qubit [36], a_0 , is to make the error $Z_1Z_7 = \bar{Z}_1\bar{Z}_2$ detectable. Similarly, the flag qubits a_1 and a_2 catch the errors Z_2Z_7 , Z_3Z_6 and Z_4Z_6 .

IV. DEMONSTRATION RESULTS

We investigate the performance of circuits comprised of three parts: state preparation, a transversal logical gate, and logical measurement.

For the state preparation part, we consider either $|\text{GHZ}\rangle$ or $|+++ \rangle$ state preparation, using the circuits described in Section III. For the logical gate part, we consider each of the distinct products of the transversal logical CCZ, CZ_{12} , CZ_{02} and CZ_{01} gates available in the $[[8,3,2]]$ code, along with the logical identity gate implemented as a ‘no operation’. For the logical measurement part, we consider transversal Z basis and X basis measurements. In the encoded case, the fault-tolerant measurement involves post-selection and we provide the post-selection rates for each of the demonstrations in Appendix A 2.

We test these circuits on two quantum computers: `ibmq_mumbai`, a 27-qubit device developed by IBM [37], and `ionq-11q`, an 11-qubit device developed by IonQ [13].

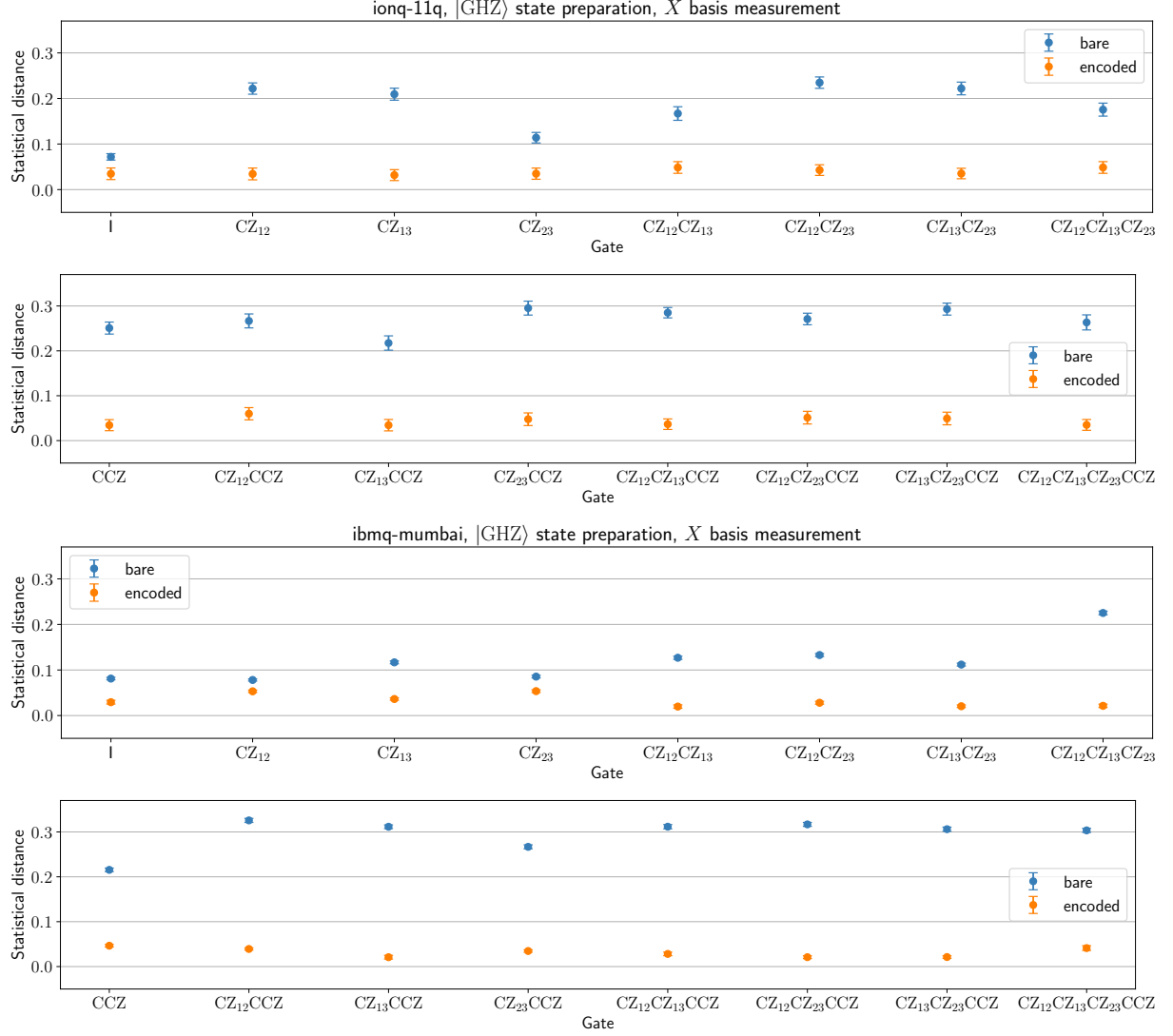


Figure 4. Performance of bare (non-encoded) and encoded versions of circuits for preparing states of the form $g|\text{GHZ}\rangle$, where g is a transversal gate of the $[[8,3,2]]$ code. In each case, we measure the qubits in the X basis and we plot the statistical distance of the observed measurement distribution from the ideal distribution. The upper two plots show the data for `ionq-11q`, where we ran 1024 shots for each circuit, and the lower two plots show the data for `ibmq_mumbai` where we ran 10,000 shots for each circuit. In both cases, the error bars are calculated using bootstrap resampling.

The IonQ device has all-to-all qubit connectivity, whereas the IBM device has “heavy-hexagon” qubit connectivity [38]; see Appendix B more details on the devices and their characteristics at the time of the demonstrations. We only consider $|\text{GHZ}\rangle$ state preparation on the IBM device, as our circuit for preparing logical $|+++ \rangle$ states (Fig. 3) does not respect the connectivity constraints of the IBM device and would therefore require SWAP gates to implement, meaning that our error analysis is no longer valid. We leave open the possibility of finding a fault-tolerant circuit for preparing logical $|+++ \rangle$ states on the IBM device. We compare the performance of the encoded circuits against the performance of the bare (no encoding) circuits, using the statistical distance of the

output distribution from the ideal output distribution as our metric. The data and analysis code is available at [39].

We show the results for $|\text{GHZ}\rangle$ state preparation and X basis measurement in Fig. 4. For both devices and for every transversal gate, we observe improved performance of the encoded version of the circuit. The results for Z basis measurement are qualitatively similar; see Appendix A 1.

We show the results for $|+++ \rangle$ state preparation and X basis measurement in Fig. 5. The bare version of the circuit performs better for transversal Clifford gates, whereas the encoded version performs better for transversal non-Clifford gates. Notably, we observe lower statis-

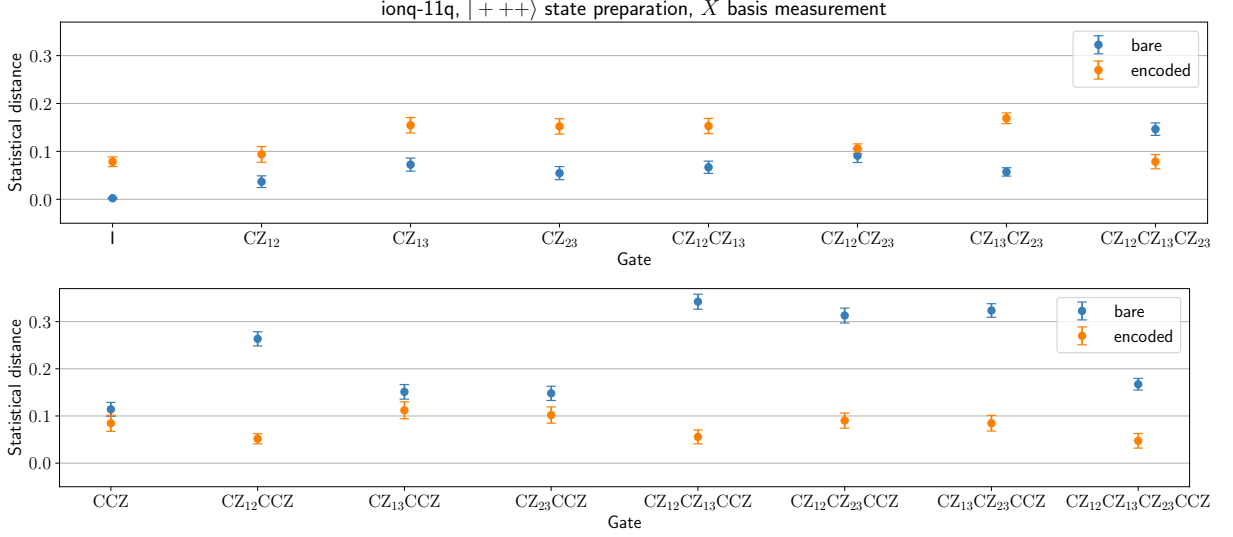


Figure 5. Performance of bare (non-encoded) and encoded versions of circuits for preparing states of the form $g|+++ \rangle$, where g is a transversal gate of the $[[8,3,2]]$ code. In each case, we measure the qubits in the X basis and we plot the statistical distance of the observed measurement distribution from the ideal distribution. Each data point represents 1024 shots of the circuit performed on ionq-11q, and we use bootstrap resampling to calculate the error bars.

tical distances for the preparation of the encoded magic state $\text{CCZ}|+++ \rangle$. We can attribute the difference between the results for Clifford and non-Clifford gates to the compilation of the three-qubit CCZ gate into a circuit involving multiple two-qubit gates on the IonQ device [40]. And the discrepancy between the results for $|+++ \rangle$ and $|\text{GHZ}\rangle$ state preparation is expected, given that the bare circuit for preparing the former requires only single-qubit gates and the latter requires two entangling gates. We again relegate the results for Z basis measurement to Appendix A 1, as they are qualitatively similar to the results for X basis measurement.

V. DISCUSSION

We have shown that using the $[[8,3,2]]$ code allows us to prepare certain (encoded) states more accurately (as measured by the statistical distance) than using the native gates to prepare the same (non-encoded) states. We observe this advantage across a range of circuits on two different hardware platforms: IBM’s superconducting qubits and IonQ’s trapped-ion qubits. The all-to-all connectivity of the IonQ device that we used enabled us to run more circuits fault-tolerantly than we could on the IBM device. In particular, we were able to interrogate the performance of the $[[8,3,2]]$ code for preparing magic states of the form $g|+++ \rangle$, where $g \in \text{CCZ} \times \{I, \text{CZ}_{12}, \text{CZ}_{13}, \text{CZ}_{23}\}$. We observe an improved performance for the encoded version of circuits for preparing these states, illustrating the utility of codes like the $[[8,3,2]]$ code, where multi-qubit non-Clifford gates can be applied using single-qubit operations.

The $[[8,3,2]]$ is one example of a family of codes, known as generalized triorthogonal codes [41–43], with transversal multi-qubit Z rotations implemented by single-qubit gates. In future it would be interesting to test the performance of larger codes in this family with higher distance. For example, Ref. [43] gives a $[[64,6,4]]$ code with a transversal $\text{CCZ}^{\otimes 2}$ gate and it is possible that smaller examples could be found using the techniques of [44–46]. In addition, 3D color codes [47–49] are also generalized triorthogonal codes and therefore our approach could be extended to the error-correcting regime by exchanging the $[[8,3,2]]$ code for a color code with larger distance (for concrete examples see [50, 51]).

As with any stabilizer code, the transversal gates of the $[[8,3,2]]$ code do not form a universal set of gates. Therefore, in order to use the $[[8,3,2]]$ code or a similar code to implement an actual quantum algorithm, we would need to supplement the transversal gates with additional fault-tolerant gates in order to obtain a universal gate set. One possibility worth considering would be to explore the implementation of logical gates via permutations of the physical qubits [52, 53], which can be fault-tolerant if implemented by qubit relabelling or physically moving the qubits.

ACKNOWLEDGEMENTS

Research at Perimeter Institute is supported in part by the Government of Canada through the Department of Innovation, Science and Economic Development Canada and by the Province of Ontario through the Ministry of Colleges and Universities. We acknowledge the support

of the Natural Sciences and Engineering Research Council of Canada (NSERC). We thank IonQ for giving us access to their hardware through the IonQ Research Credits Program. We acknowledge CMC Microsystems for facilitating this research, specifically through their mem-

ber access to the IBM Quantum Hub at PINQ². We thank Benjamin Brown, Ben Criger, Joel Klassen and James Seddon for useful discussions. We thank Raymond Laflamme for comments on an earlier version of this manuscript.

-
- [1] P. W. Shor, Phys. Rev. A **52**, R2493 (1995).
 - [2] A. M. Steane, Phys. Rev. Lett. **77**, 793 (1996).
 - [3] I. L. Chuang and R. Laflamme, arXiv preprint (1995), arXiv:quant-ph/9511003.
 - [4] P. Shor, in *Proceedings of 37th Conference on Foundations of Computer Science* (1996), pp. 56–65, ISBN 978-0-8186-7594-2.
 - [5] B. Eastin and E. Knill, Phys. Rev. Lett. **102**, 110502 (2009).
 - [6] G. Nebe, E. M. Rains, and N. J. A. Sloane, Designs, Codes and Cryptography **24**, 99 (2001).
 - [7] S. Bravyi and A. Kitaev, Phys. Rev. A **71**, 022316 (2005).
 - [8] E. Knill, arXiv preprint (2004), arXiv:quant-ph/0402171.
 - [9] S. Bravyi and J. Haah, Phys. Rev. A **86**, 052329 (2012).
 - [10] A. Kubica, B. Yoshida, and F. Pastawski, New J. Phys. **17**, 083026 (2015).
 - [11] E. Campbell, *The smallest interesting colour code*, <https://earlthcampbell.com/2016/09/26/the-smallest-interesting-colour-code/> (2016).
 - [12] C. J. Ballance, T. P. Harty, N. M. Linke, M. A. Sepiol, and D. M. Lucas, Phys. Rev. Lett. **117**, 060504 (2016).
 - [13] K. Wright, K. M. Beck, S. Debnath, J. M. Amini, Y. Nam, N. Grzesiak, J.-S. Chen, N. C. Pientti, M. Chmielewski, C. Collins, et al., Nat. Commun. **10**, 5464 (2019).
 - [14] P. Jurcevic, A. Javadi-Abhari, L. S. Bishop, I. Lauer, D. F. Bogorin, M. Brink, L. Capelluto, O. Günlük, T. Itoko, N. Kanazawa, et al., Quantum Sci. Technol. **6**, 025020 (2021).
 - [15] Y. Wu, W.-S. Bao, S. Cao, F. Chen, M.-C. Chen, X. Chen, T.-H. Chung, H. Deng, Y. Du, D. Fan, et al., Phys. Rev. Lett. **127**, 180501 (2021).
 - [16] W. Huang, C. H. Yang, K. W. Chan, T. Tanttu, B. Hensen, R. C. C. Leon, M. A. Fogarty, J. C. C. Hwang, F. E. Hudson, K. M. Itoh, et al., Nature **569**, 532 (2019).
 - [17] S. A. Moses, C. H. Baldwin, M. S. Allman, R. Ancona, L. Ascarrunz, C. Barnes, J. Bartolotta, B. Bjork, P. Blanchard, M. Bohn, et al., arXiv preprint (2023), arXiv:2305.03828.
 - [18] D. Gottesman, arXiv preprint (2016), arXiv:1610.03507.
 - [19] A. M. Souza, J. Zhang, C. A. Ryan, and R. Laflamme, Nat. Commun. **2**, 169 (2011).
 - [20] J. Zhang, R. Laflamme, and D. Suter, Phys. Rev. Lett. **109**, 100503 (2012).
 - [21] D. Nigg, M. Mueller, E. A. Martinez, P. Schindler, M. Hennrich, T. Monz, M. A. Martin-Delgado, and R. Blatt, Science **345**, 302 (2014), arXiv:1403.5426.
 - [22] L. Egan, D. M. Debroy, C. Noel, A. Risinger, D. Zhu, D. Biswas, M. Newman, M. Li, K. R. Brown, M. Cetina, et al., arXiv preprint (2021), arXiv:2009.11482.
 - [23] L. Postler, S. Heuβen, I. Pogorelov, M. Rispler, T. Feldker, M. Meth, C. D. Marciniak, R. Stricker, M. Ringbauer, R. Blatt, et al., Nature **605**, 675 (2022).
 - [24] C. Ryan-Anderson, N. C. Brown, M. S. Allman, B. Arkin, G. Asa-Attuah, C. Baldwin, J. Berg, J. G. Bohnet, S. Braxton, N. Burdick, et al., arXiv preprint (2022), arXiv:2208.01863.
 - [25] C. Vuillot, Quantum Inf. Comput. **18**, 0949 (2018).
 - [26] R. Harper and S. T. Flammia, Phys. Rev. Lett. **122**, 080504 (2019).
 - [27] R. S. Gupta, N. Sundaresan, T. Alexander, C. J. Wood, S. T. Merkel, M. B. Healy, M. Hillenbrand, T. Jochym-O'Connor, J. R. Wootton, T. J. Yoder, et al., arXiv preprint (2023), arXiv:2305.13581.
 - [28] V. Vedral, A. Barenco, and A. Ekert, Phys. Rev. A **54**, 147 (1996).
 - [29] C. Gidney, Quantum **2**, 74 (2018).
 - [30] P. W. Shor, SIAM J. Comput. **26**, 1484 (1997).
 - [31] C. Gidney and M. Ekerå, Quantum **5**, 433 (2021).
 - [32] D. Gottesman, Ph.D. thesis, Caltech (1997), arXiv:quant-ph/9705052.
 - [33] A. R. Calderbank and P. W. Shor, Phys. Rev. A **54**, 1098 (1996).
 - [34] A. M. Steane, Proc. R. Soc. Lond. A **452**, 2551 (1996).
 - [35] M. A. Nielsen and I. L. Chuang, *Quantum Computation and Quantum Information: 10th Anniversary Edition* (Cambridge University Press, 2010).
 - [36] R. Chao and B. W. Reichardt, Phys. Rev. Lett. **121**, 050502 (2018).
 - [37] *IBM Quantum*, <https://quantum-computing.ibm.com/>.
 - [38] J. B. Hertzberg, E. J. Zhang, S. Rosenblatt, E. Magesan, J. A. Smolin, J.-B. Yau, V. P. Adiga, M. Sandberg, M. Brink, J. M. Chow, et al., npj Quantum Inf. **7**, 129 (2021).
 - [39] M. Vasmer, *Data analysis for "implementing fault-tolerant non-clifford gates using the $[[8,3,2]]$ color code"*, <https://github.com/MikeVasmer/832-code>.
 - [40] *Getting started with Native Gates*, <https://ionq.com/docs/getting-started-with-native-gates>.
 - [41] E. T. Campbell and M. Howard, Phys. Rev. Lett. **118**, 060501 (2017).
 - [42] E. T. Campbell and M. Howard, Phys. Rev. A **95**, 022316 (2017).
 - [43] J. Haah and M. B. Hastings, Quantum **2**, 71 (2018).
 - [44] S. Nezami and J. Haah, Phys. Rev. A **106**, 012437 (2022).
 - [45] J. Hu, Q. Liang, and R. Calderbank, Quantum **6**, 802 (2022).
 - [46] M. A. Webster, A. O. Quintavalle, and S. D. Bartlett, arXiv preprint (2023), arXiv:2303.15615.
 - [47] H. Bombin and M. A. Martin-Delgado, Phys. Rev. Lett. **98**, 160502 (2007).
 - [48] H. Bombín, New Journal of Physics **17**, 083002 (2015).
 - [49] A. Kubica and M. E. Beverland, Phys. Rev. A **91**, 032330 (2015).
 - [50] M. Vasmer and D. E. Browne, Phys. Rev. A **100**, 012312 (2019).

- [51] M. Vasmer and A. Kubica, PRX Quantum **3**, 030319 (2022).
 [52] M. Grassl and M. Roetteler, in *2013 IEEE International Symposium on Information Theory* (2013), pp. 534–538.
 [53] R. Chao and B. W. Reichardt, npj Quantum Inf. **4**, 42 (2018).

Appendix A: Additional demonstration results

1. Logical Z basis measurement results

For the demonstrations with $|+++ \rangle$ state preparation and Z basis measurement, we observe improved performance for the encoded circuits containing a transversal non-Clifford gate; see Fig. 6. And for the demonstrations with $|\text{GHZ}\rangle$ state preparation and Z basis measurement, we observe improved performance for all of the encoded circuits; see Fig. 7. We note that in these cases the gates have no effect on the expected output measurement distribution, as the gates commute with the measurements.

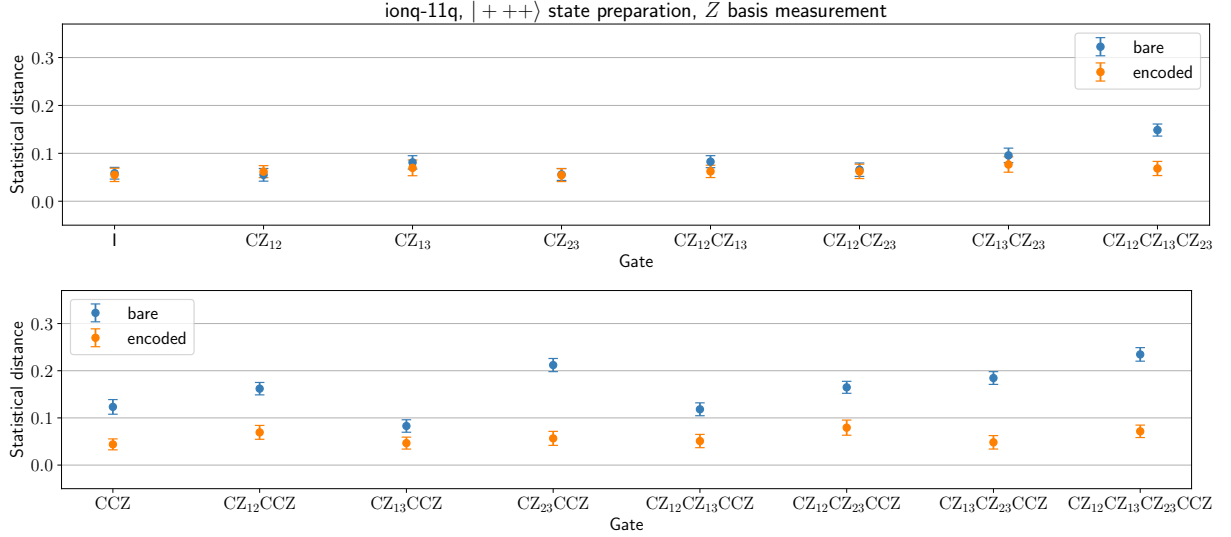


Figure 6. Performance of bare (non-encoded) and encoded versions of circuits for preparing states of the form $g|+++ \rangle$, where g is a transversal gate of the $[[8,3,2]]$ code. In each case, we measure the qubits in the Z basis and we plot the statistical distance of the observed measurement distribution from the ideal distribution. Each data point represents 1024 shots of the circuit performed on *ionq-11q*, and we use bootstrap resampling to calculate the error bars.

2. Post-selection rates

In this appendix, we provide the post-selection rates (proportion of accepted shots) for our demonstrations. Two-qubit gates and measurements are the noisiest operations in superconducting and trapped-ion devices [13, 14], hence we can approximate the error model in these devices with ideal state preparation and one-qubit gates, but noisy two-qubit gates and measurements (1% error rate). Suppose that any two-qubit gate error or measurement error causes us to discard the run, then (to first order) we would expect a post-selection rate of $1 - 0.01(n_m + n_g)$, where n_m is the number of measurements and n_g is the number of two-qubit gates. By counting the relevant locations in Figs. 2 and 3, we therefore estimate a post-selection rate of 69% and 86% for the circuits with $|+++ \rangle$ and $|\text{GHZ}\rangle$ state preparation, respectively. These estimates are reasonably close to the values we observe in our demonstrations; see Tables I to III.

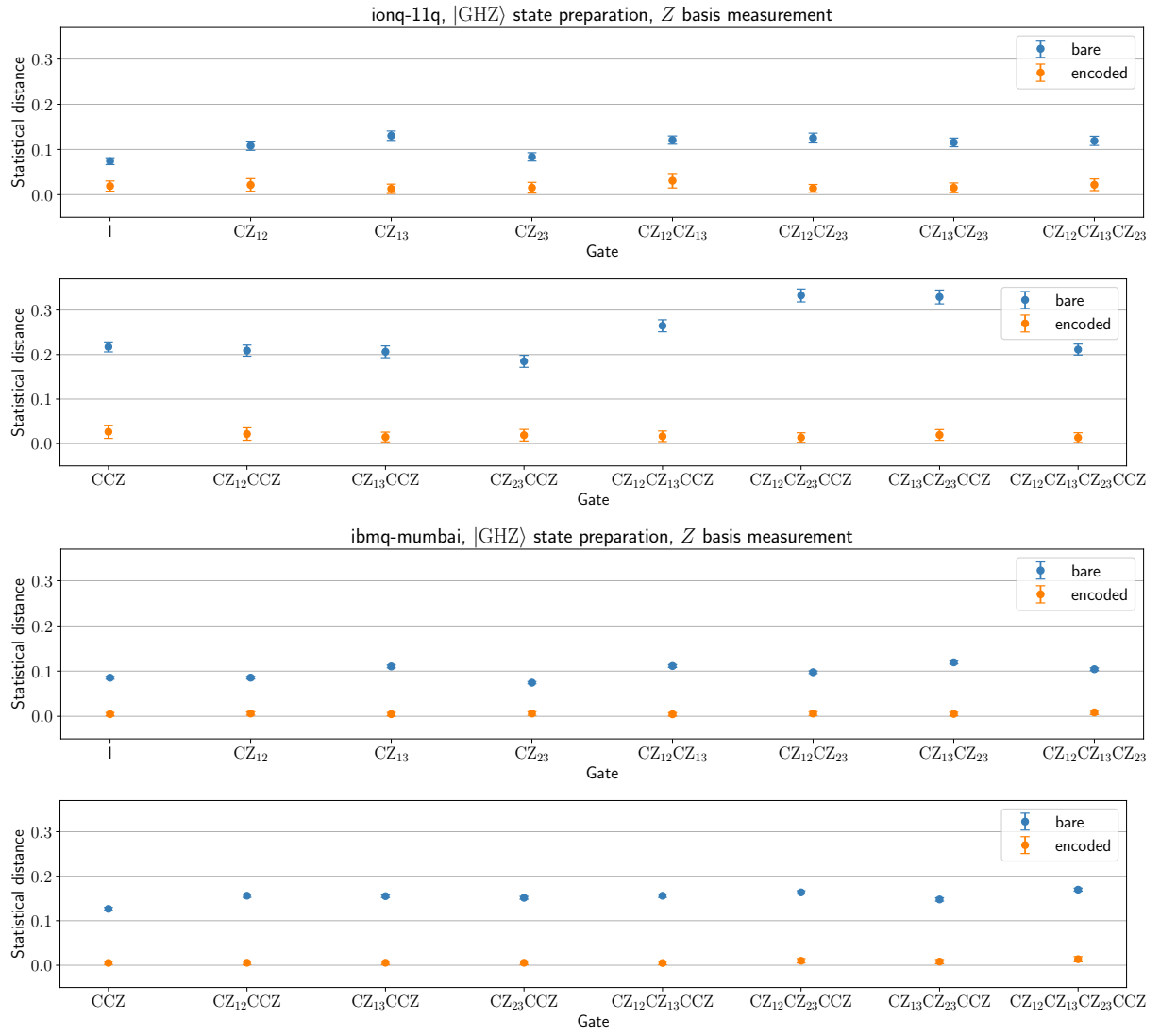


Figure 7. Performance of bare (non-encoded) and encoded versions of circuits for preparing states of the form $g|GHZ\rangle$, where g is a transversal gate of the $[[8,3,2]]$ code. In each case, we measure the qubits in the Z basis and we plot the statistical distance of the observed measurement distribution from the ideal distribution. The upper two plots show the data for **ionq-11q**, where we ran 1024 shots for each circuit, and the lower two plots show the data for **ibmq_mumbai** where we ran 10,000 shots for each circuit. In both cases, the error bars are calculated using bootstrap resampling.

State	Gate	Measurement	Device	Post-selection rate
$ +++ \rangle$	I	X basis	ionq-11q	78%
$ +++ \rangle$	CZ_{12}	X basis	ionq-11q	78%
$ +++ \rangle$	CZ_{13}	X basis	ionq-11q	69%
$ +++ \rangle$	$CZ_{12}CZ_{13}$	X basis	ionq-11q	76%
$ +++ \rangle$	CZ_{23}	X basis	ionq-11q	80%
$ +++ \rangle$	$CZ_{12}CZ_{23}$	X basis	ionq-11q	77%
$ +++ \rangle$	$CZ_{13}CZ_{23}$	X basis	ionq-11q	79%
$ +++ \rangle$	$CZ_{12}CZ_{13}CZ_{23}$	X basis	ionq-11q	80%
$ +++ \rangle$	CCZ	X basis	ionq-11q	75%
$ +++ \rangle$	$CZ_{12}CCZ$	X basis	ionq-11q	81%
$ +++ \rangle$	$CZ_{13}CCZ$	X basis	ionq-11q	74%
$ +++ \rangle$	$CZ_{12}CZ_{13}CCZ$	X basis	ionq-11q	84%
$ +++ \rangle$	$CZ_{23}CCZ$	X basis	ionq-11q	75%
$ +++ \rangle$	$CZ_{12}CZ_{23}CCZ$	X basis	ionq-11q	83%
$ +++ \rangle$	$CZ_{13}CZ_{23}CCZ$	X basis	ionq-11q	77%
$ +++ \rangle$	$CZ_{12}CZ_{13}CZ_{23}CCZ$	X basis	ionq-11q	77%
$ +++ \rangle$	I	Z basis	ionq-11q	73%
$ +++ \rangle$	CZ_{12}	Z basis	ionq-11q	78%
$ +++ \rangle$	CZ_{13}	Z basis	ionq-11q	71%
$ +++ \rangle$	$CZ_{12}CZ_{13}$	Z basis	ionq-11q	74%
$ +++ \rangle$	CZ_{23}	Z basis	ionq-11q	72%
$ +++ \rangle$	$CZ_{12}CZ_{23}$	Z basis	ionq-11q	72%
$ +++ \rangle$	$CZ_{13}CZ_{23}$	Z basis	ionq-11q	73%
$ +++ \rangle$	$CZ_{12}CZ_{13}CZ_{23}$	Z basis	ionq-11q	71%
$ +++ \rangle$	CCZ	Z basis	ionq-11q	74%
$ +++ \rangle$	$CZ_{12}CCZ$	Z basis	ionq-11q	74%
$ +++ \rangle$	$CZ_{13}CCZ$	Z basis	ionq-11q	70%
$ +++ \rangle$	$CZ_{12}CZ_{13}CCZ$	Z basis	ionq-11q	74%
$ +++ \rangle$	$CZ_{23}CCZ$	Z basis	ionq-11q	72%
$ +++ \rangle$	$CZ_{12}CZ_{23}CCZ$	Z basis	ionq-11q	73%
$ +++ \rangle$	$CZ_{13}CZ_{23}CCZ$	Z basis	ionq-11q	74%
$ +++ \rangle$	$CZ_{12}CZ_{13}CZ_{23}CCZ$	Z basis	ionq-11q	73%

Table I. Post-selection rates for the results shown in Figs. 5 and 6, where the percentage indicates the proportion of shots that were accepted. The average post-selection rate was 75%.

State	Gate	Measurement	Device	Post-selection rate
$ GHZ\rangle$	I	X basis	ionq-11q	90%
$ GHZ\rangle$	CZ_{12}	X basis	ionq-11q	86%
$ GHZ\rangle$	CZ_{13}	X basis	ionq-11q	90%
$ GHZ\rangle$	$CZ_{12}CZ_{13}$	X basis	ionq-11q	78%
$ GHZ\rangle$	CZ_{23}	X basis	ionq-11q	83%
$ GHZ\rangle$	$CZ_{12}CZ_{23}$	X basis	ionq-11q	81%
$ GHZ\rangle$	$CZ_{13}CZ_{23}$	X basis	ionq-11q	82%
$ GHZ\rangle$	$CZ_{12}CZ_{13}CZ_{23}$	X basis	ionq-11q	79%
$ GHZ\rangle$	CCZ	X basis	ionq-11q	80%
$ GHZ\rangle$	$CZ_{12}CCZ$	X basis	ionq-11q	78%
$ GHZ\rangle$	$CZ_{13}CCZ$	X basis	ionq-11q	82%
$ GHZ\rangle$	$CZ_{12}CZ_{13}CCZ$	X basis	ionq-11q	87%
$ GHZ\rangle$	$CZ_{23}CCZ$	X basis	ionq-11q	83%
$ GHZ\rangle$	$CZ_{12}CZ_{23}CCZ$	X basis	ionq-11q	83%
$ GHZ\rangle$	$CZ_{13}CZ_{23}CCZ$	X basis	ionq-11q	82%
$ GHZ\rangle$	$CZ_{12}CZ_{13}CZ_{23}CCZ$	X basis	ionq-11q	84%
$ GHZ\rangle$	I	Z basis	ionq-11q	86%
$ GHZ\rangle$	CZ_{12}	Z basis	ionq-11q	81%
$ GHZ\rangle$	CZ_{13}	Z basis	ionq-11q	84%
$ GHZ\rangle$	$CZ_{12}CZ_{13}$	Z basis	ionq-11q	85%
$ GHZ\rangle$	CZ_{23}	Z basis	ionq-11q	81%
$ GHZ\rangle$	$CZ_{12}CZ_{23}$	Z basis	ionq-11q	90%
$ GHZ\rangle$	$CZ_{13}CZ_{23}$	Z basis	ionq-11q	84%
$ GHZ\rangle$	$CZ_{12}CZ_{13}CZ_{23}$	Z basis	ionq-11q	81%
$ GHZ\rangle$	CCZ	Z basis	ionq-11q	86%
$ GHZ\rangle$	$CZ_{12}CCZ$	Z basis	ionq-11q	80%
$ GHZ\rangle$	$CZ_{13}CCZ$	Z basis	ionq-11q	87%
$ GHZ\rangle$	$CZ_{12}CZ_{13}CCZ$	Z basis	ionq-11q	75%
$ GHZ\rangle$	$CZ_{23}CCZ$	Z basis	ionq-11q	74%
$ GHZ\rangle$	$CZ_{12}CZ_{23}CCZ$	Z basis	ionq-11q	83%
$ GHZ\rangle$	$CZ_{13}CZ_{23}CCZ$	Z basis	ionq-11q	75%
$ GHZ\rangle$	$CZ_{12}CZ_{13}CZ_{23}CCZ$	Z basis	ionq-11q	85%

Table II. Post-selection rates for the results shown in Figs. 4 and 7 for the IonQ device, where the percentage indicates the proportion of shots that were accepted. The average post-selection rate was 83%.

State	Gate	Measurement	Device	Post-selection rate
$ \text{GHZ}\rangle$	I	X basis	ibmq_mumbai	76%
$ \text{GHZ}\rangle$	CZ_{12}	X basis	ibmq_mumbai	69%
$ \text{GHZ}\rangle$	CZ_{13}	X basis	ibmq_mumbai	72%
$ \text{GHZ}\rangle$	$CZ_{12}CZ_{13}$	X basis	ibmq_mumbai	79%
$ \text{GHZ}\rangle$	CZ_{23}	X basis	ibmq_mumbai	69%
$ \text{GHZ}\rangle$	$CZ_{12}CZ_{23}$	X basis	ibmq_mumbai	76%
$ \text{GHZ}\rangle$	$CZ_{13}CZ_{23}$	X basis	ibmq_mumbai	78%
$ \text{GHZ}\rangle$	$CZ_{12}CZ_{13}CZ_{23}$	X basis	ibmq_mumbai	80%
$ \text{GHZ}\rangle$	CCZ	X basis	ibmq_mumbai	72%
$ \text{GHZ}\rangle$	$CZ_{12}CCZ$	X basis	ibmq_mumbai	73%
$ \text{GHZ}\rangle$	$CZ_{13}CCZ$	X basis	ibmq_mumbai	79%
$ \text{GHZ}\rangle$	$CZ_{12}CZ_{13}CCZ$	X basis	ibmq_mumbai	76%
$ \text{GHZ}\rangle$	$CZ_{23}CCZ$	X basis	ibmq_mumbai	73%
$ \text{GHZ}\rangle$	$CZ_{12}CZ_{23}CCZ$	X basis	ibmq_mumbai	79%
$ \text{GHZ}\rangle$	$CZ_{13}CZ_{23}CCZ$	X basis	ibmq_mumbai	79%
$ \text{GHZ}\rangle$	$CZ_{12}CZ_{13}CZ_{23}CCZ$	X basis	ibmq_mumbai	72%
$ \text{GHZ}\rangle$	I	Z basis	ibmq_mumbai	74%
$ \text{GHZ}\rangle$	CZ_{12}	Z basis	ibmq_mumbai	70%
$ \text{GHZ}\rangle$	CZ_{13}	Z basis	ibmq_mumbai	74%
$ \text{GHZ}\rangle$	$CZ_{12}CZ_{13}$	Z basis	ibmq_mumbai	77%
$ \text{GHZ}\rangle$	CZ_{23}	Z basis	ibmq_mumbai	71%
$ \text{GHZ}\rangle$	$CZ_{12}CZ_{23}$	Z basis	ibmq_mumbai	71%
$ \text{GHZ}\rangle$	$CZ_{13}CZ_{23}$	Z basis	ibmq_mumbai	75%
$ \text{GHZ}\rangle$	$CZ_{12}CZ_{13}CZ_{23}$	Z basis	ibmq_mumbai	73%
$ \text{GHZ}\rangle$	CCZ	Z basis	ibmq_mumbai	76%
$ \text{GHZ}\rangle$	$CZ_{12}CCZ$	Z basis	ibmq_mumbai	78%
$ \text{GHZ}\rangle$	$CZ_{13}CCZ$	Z basis	ibmq_mumbai	78%
$ \text{GHZ}\rangle$	$CZ_{12}CZ_{13}CCZ$	Z basis	ibmq_mumbai	77%
$ \text{GHZ}\rangle$	$CZ_{23}CCZ$	Z basis	ibmq_mumbai	78%
$ \text{GHZ}\rangle$	$CZ_{12}CZ_{23}CCZ$	Z basis	ibmq_mumbai	77%
$ \text{GHZ}\rangle$	$CZ_{13}CZ_{23}CCZ$	Z basis	ibmq_mumbai	77%
$ \text{GHZ}\rangle$	$CZ_{12}CZ_{13}CZ_{23}CCZ$	Z basis	ibmq_mumbai	71%

Table III. Post-selection rates for the results shown in Figs. 4 and 7 for the IBM device, where the percentage indicates the proportion of shots that were accepted. The average post-selection rate was 75%.

Appendix B: Additional hardware details

1. IBM

The layout of the `ibmq_mumbai` device is shown in Fig. 8. The demonstrations were carried out on 14/04/23. The 1-qubit and 2-qubit gate characterization data provided by IBM for this date are given in Tables IV and V. The qubit characterization data provided by IBM for this date are given in Table VI and the qubit reset time was 3612 ns for all qubits.

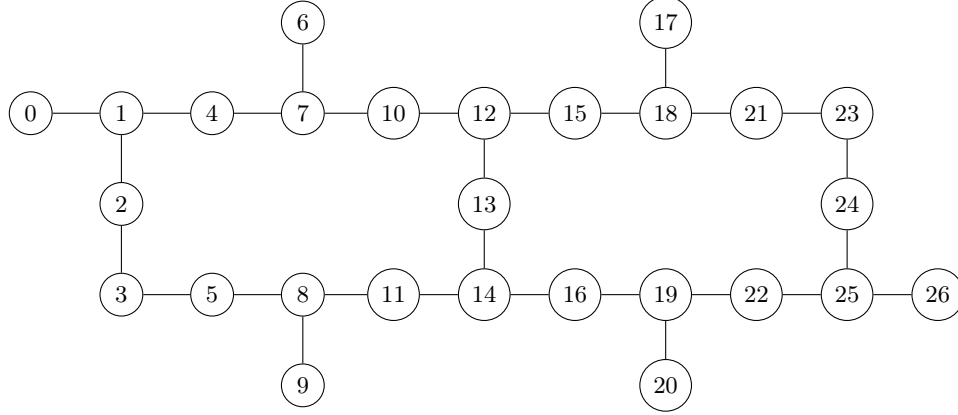


Figure 8. Layout of the `ibmq_mumbai` device. Vertices represent qubits and edges represent the availability of entangling gates between the two endpoints. The mapping from the qubits of the $[[8,3,2]]$ code to the qubits of the device was $(q_0, 7)$, $(q_1, 4)$, $(q_2, 1)$, $(q_3, 10)$, $(q_4, 2)$, $(q_5, 12)$, $(q_6, 13)$, $(q_7, 3)$.

2. IonQ

The `ionq-11q` device has 11 qubits and all-to-all connectivity. The characterization data provided by IonQ for the dates that the demonstrations were carried out are given in Table VII.

Qubit	Gate	Error	Time
0	I, X, \sqrt{X}	0.0002951	35.56 ns
1	I, X, \sqrt{X}	0.0001877	35.56 ns
2	I, X, \sqrt{X}	0.0001816	35.56 ns
3	I, X, \sqrt{X}	0.0002697	35.56 ns
4	I, X, \sqrt{X}	0.0003707	35.56 ns
5	I, X, \sqrt{X}	0.0002801	35.56 ns
6	I, X, \sqrt{X}	0.000267	35.56 ns
7	I, X, \sqrt{X}	0.0001768	35.56 ns
8	I, X, \sqrt{X}	0.0001585	35.56 ns
9	I, X, \sqrt{X}	0.0003164	35.56 ns
10	I, X, \sqrt{X}	0.0002868	35.56 ns
11	I, X, \sqrt{X}	0.0002381	35.56 ns
12	I, X, \sqrt{X}	0.0001866	35.56 ns
13	I, X, \sqrt{X}	0.0001609	35.56 ns
14	I, X, \sqrt{X}	0.000182	35.56 ns
15	I, X, \sqrt{X}	0.0004084	35.56 ns
16	I, X, \sqrt{X}	0.0001818	35.56 ns
17	I, X, \sqrt{X}	0.002198	35.56 ns
18	I, X, \sqrt{X}	0.0002243	35.56 ns
19	I, X, \sqrt{X}	0.0001976	35.56 ns
20	I, X, \sqrt{X}	0.0002066	35.56 ns
21	I, X, \sqrt{X}	0.0004652	35.56 ns
22	I, X, \sqrt{X}	0.000166	35.56 ns
23	I, X, \sqrt{X}	0.0003324	35.56 ns
24	I, X, \sqrt{X}	0.0001602	35.56 ns
25	I, X, \sqrt{X}	0.0002232	35.56 ns
26	I, X, \sqrt{X}	0.0002714	35.56 ns

Table IV. 1-qubit gate characterization data for ibmq_mumbai on 14/04/23.

Qubits	Gate	Error	Time
3,2	CNOT	0.008789	433.8 ns
2,3	CNOT	0.008789	469.3 ns
14,11	CNOT	0.005348	391.1 ns
11,14	CNOT	0.005348	426.7 ns
5,8	CNOT	0.01016	604.4 ns
8,5	CNOT	0.01016	640.0 ns
12,13	CNOT	0.00516	547.6 ns
13,12	CNOT	0.00516	583.1 ns
13,14	CNOT	0.004559	320.0 ns
14,13	CNOT	0.004559	355.6 ns
22,19	CNOT	0.004825	327.1 ns
19,22	CNOT	0.004825	362.7 ns
3,5	CNOT	0.01117	476.4 ns
5,3	CNOT	0.01117	512.0 ns
18,21	CNOT	0.01269	497.8 ns
21,18	CNOT	0.01269	533.3 ns
25,22	CNOT	0.005982	448.0 ns
22,25	CNOT	0.005982	483.6 ns
2,1	CNOT	0.01161	704.0 ns
1,2	CNOT	0.01161	739.6 ns
8,11	CNOT	0.01248	604.4 ns
11,8	CNOT	0.01248	640.0 ns
10,12	CNOT	0.007643	604.4 ns
12,10	CNOT	0.007643	640.0 ns
10,7	CNOT	0.007437	398.2 ns
7,10	CNOT	0.007437	433.8 ns
20,19	CNOT	0.005657	369.8 ns
19,20	CNOT	0.005657	405.3 ns
23,21	CNOT	0.008342	362.7 ns
21,23	CNOT	0.008342	398.2 ns
6,7	CNOT	0.007037	248.9 ns
7,6	CNOT	0.007037	284.4 ns
17,18	CNOT	0.01205	248.9 ns
18,17	CNOT	0.01205	284.4 ns
4,7	CNOT	0.009587	604.4 ns
7,4	CNOT	0.009587	640.0 ns
8,9	CNOT	0.008003	604.4 ns
9,8	CNOT	0.008003	640.0 ns
16,19	CNOT	0.01609	682.7 ns
19,16	CNOT	0.01609	718.2 ns
24,23	CNOT	0.01297	604.4 ns
23,24	CNOT	0.01297	640.0 ns
4,1	CNOT	0.006135	312.9 ns
1,4	CNOT	0.006135	348.4 ns
15,18	CNOT	0.006877	305.8 ns
18,15	CNOT	0.006877	341.3 ns
16,14	CNOT	0.005754	291.6 ns
14,16	CNOT	0.005754	327.1 ns
26,25	CNOT	0.006879	312.9 ns
25,26	CNOT	0.006879	348.4 ns
0,1	CNOT	0.007626	419.6 ns
1,0	CNOT	0.007626	455.1 ns
15,12	CNOT	0.006138	369.8 ns
12,15	CNOT	0.006138	405.3 ns
24,25	CNOT	0.007386	433.8 ns
25,24	CNOT	0.007386	469.3 ns

Table V. 2-qubit gate characterization data for ibmq_mumbai on 14/04/23.

Qubit	T_1	T_2	Frequency	Anharmonicity	Readout error	$p(0 1)$	$p(1 0)$	Readout time
0	100.5 μ s	125.9 μ s	5.071 GHz	-0.3285 GHz	0.0435	0.0714	0.0156	3576 ns
1	116.4 μ s	163.8 μ s	4.93 GHz	-0.3313 GHz	0.0401	0.0476	0.0326	3576 ns
2	94.52 μ s	114.8 μ s	4.67 GHz	-0.3369 GHz	0.0153	0.0206	0.01	3576 ns
3	103.2 μ s	168.3 μ s	4.889 GHz	-0.3312 GHz	0.057	0.0622	0.0518	3576 ns
4	105.9 μ s	47.41 μ s	5.021 GHz	-0.3302 GHz	0.03	0.0424	0.0176	3576 ns
5	86.9 μ s	151.6 μ s	4.969 GHz	-0.3298 GHz	0.1603	0.178	0.1426	3576 ns
6	122.5 μ s	81.42 μ s	4.966 GHz	-0.3293 GHz	0.0169	0.0236	0.0102	3576 ns
7	125.2 μ s	164.3 μ s	4.894 GHz	-0.331 GHz	0.0162	0.0232	0.0092	3576 ns
8	212.2 μ s	256.6 μ s	4.792 GHz	-0.3326 GHz	0.018	0.0192	0.0168	3576 ns
9	149.8 μ s	119.8 μ s	4.955 GHz	-0.3306 GHz	0.0119	0.0184	0.0054	3576 ns
10	99.87 μ s	115.1 μ s	4.959 GHz	-0.3309 GHz	0.0211	0.0288	0.0134	3576 ns
11	148.1 μ s	137.1 μ s	4.666 GHz	-0.3326 GHz	0.032	0.0422	0.0218	3576 ns
12	151.6 μ s	249.3 μ s	4.743 GHz	-0.333 GHz	0.0348	0.0414	0.0282	3576 ns
13	192.4 μ s	236.7 μ s	4.889 GHz	-0.3281 GHz	0.0124	0.0184	0.0064	3576 ns
14	156.7 μ s	223.5 μ s	4.78 GHz	-0.3326 GHz	0.0214	0.0276	0.0152	3576 ns
15	111.2 μ s	36.64 μ s	4.858 GHz	-0.3332 GHz	0.024	0.0364	0.0116	3576 ns
16	131.2 μ s	187.7 μ s	4.98 GHz	-0.3299 GHz	0.0634	0.075	0.0518	3576 ns
17	63.8 μ s	114.2 μ s	5.003 GHz	-0.3299 GHz	0.0206	0.0314	0.0098	3576 ns
18	132.7 μ s	172.1 μ s	4.781 GHz	-0.3331 GHz	0.0787	0.0852	0.0722	3576 ns
19	169.2 μ s	209.2 μ s	4.81 GHz	-0.3321 GHz	0.0306	0.0316	0.0296	3576 ns
20	96.24 μ s	218.2 μ s	5.048 GHz	-0.328 GHz	0.0137	0.0226	0.0048	3576 ns
21	105.7 μ s	162.3 μ s	4.943 GHz	-0.3313 GHz	0.0418	0.0666	0.017	3576 ns
22	161.2 μ s	194.7 μ s	4.911 GHz	-0.3318 GHz	0.0145	0.0232	0.0058	3576 ns
23	102.2 μ s	166.8 μ s	4.893 GHz	-0.3315 GHz	0.0471	0.0582	0.036	3576 ns
24	139.5 μ s	41.14 μ s	4.671 GHz	-0.3359 GHz	0.0152	0.0226	0.0078	3576 ns
25	146.9 μ s	182.3 μ s	4.759 GHz	-0.3336 GHz	0.0159	0.0184	0.0134	3576 ns
26	135.8 μ s	244.6 μ s	4.954 GHz	-0.3295 GHz	0.018	0.0214	0.0146	3576 ns

Table VI. Qubit characterization data for `ibmq_mumbai` on 14/04/23. $p(i|j)$ is the probability of measuring a $|i\rangle$ state, given that a $|j\rangle$ state was prepared.

Date	1q gate fidelity	2q gate fidelity	SPAM fidelity	T_1	T_2	1q gate time	2q gate time	Readout time	Reset time
26/07/23	0.9958	0.9652	0.99752	10 000 s	0.2 s	10 μ s	200 μ s	130 μ s	20 μ s
15/08/23	0.9976	0.9906	0.99752	10 000 s	0.2 s	10 μ s	200 μ s	130 μ s	20 μ s

Table VII. Characterization data for `ionq-11q`. The demonstrations shown in Figs. 5 and 6 were conducted on 26/07/23 and the demonstrations shown in Figs. 4 and 7 were conducted on 17/08/23 (the data for 15/08/23 shown in the table is the nearest in time to when the relevant demonstrations were carried out). The fidelities are mean values. SPAM stands for state-preparation and measurement.